Title

Electric-Field-Driven Localization of Molecular Nanowires in Wafer-Scale Nanogap Electrodes.

Journal

Nano Letters, 24(33)

Authors

Wong, Han
Fischer, Felix

Publication Date

2024-08-21

DOI

10.1021/acs.nanolett.4c02329

Peer reviewed

NANO LETTERS

pubs.acs.org/NanoLett
Letter

Electric-Field-Driven Localization of Molecular Nanowires in Wafer-Scale Nanogap Electrodes

Han Xuan Wong and Felix R. Fischer*

Cite This: *Nano Lett.* 2024, 24, 10155−10160
Read Online

ACCESS | Metrics & More | Article Recommendations | Supporting Information

ABSTRACT: As integrated circuits continue to scale toward the atomic limit, bottom-up processes, such as epitaxial growth, have come to feature prominently in their fabrication. At the same time, chemistry has developed highly tunable molecular semiconductors that can perform the functions of ultimately scaled circuit components. Hybrid techniques that integrate programmable structures comprising molecular components into devices however are sorely lacking. Here we demonstrate a wafer-scale process that directs the localization of a conductive polymer, M_w = 20 kg mol^{-1} polyaniline, from dilute solutions into 50 nm vertical nanogap device architectures using electric-field-driven self-assembly. The resulting metal−polymer−metal junctions were characterized by electron microscopy, Raman spectroscopy and transport measurements demonstrating that our technique is highly selective, assembling conductive polymers only in electrically activated nanogaps. Our results represent a step toward scalable hybrid nanoelectronics that seamlessly integrate established lithographic top-down fabrication with bottom-up synthesized molecular functional circuit components.

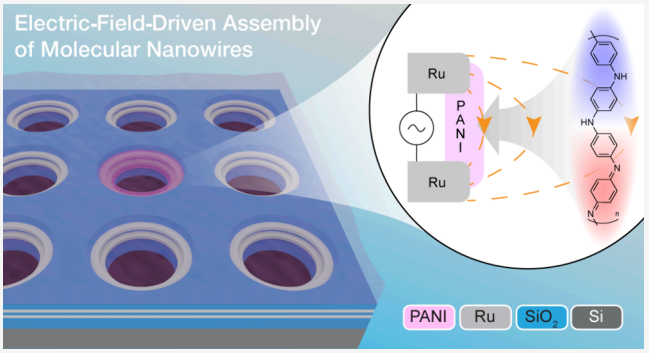

KEYWORDS: *Dielectrophoresis, Directed Assembly, Nanowires, Conductive Polymer, Molecular Electronics, Nanogap, Wafer-Scale*

Recent advances in the bottom-up synthesis and processing of low-dimensional materials with highly tunable electronic properties have reignited the prospect of hybrid nanoelectronics. Combining the scalability of top-down fabrication with the atomically precise structure of bottom-up materials could one day supplant complementary metal-oxide-semiconductor (CMOS) technology as silicon approaches its physical limits. Examples include semiconducting carbon nanotubes,[1,2] graphene nanoribbons,[3] or metal chalcogenides[4,5] as channel materials in field effect transistors (FETs). Bottom-up synthesized graphene nanoribbons in particular have been promising materials candidates that combine electronic performance with highly tunable band structures or magnetically ordered phases relevant for spintronics.[6] However, at the ultimate limit of scaling, the integration of such discrete molecular components into dense architectures requires deterministic control over position and orientation.[3] Broadly speaking, the integration challenge comprises two parts: nanogap formation and nanogap bridging.[7] In this work, we address both aspects by combining vertical nanogaps and electric-field-driven manipulation, giving access to a scalable platform capable of localizing unfunctionalized, low molecular weight conductive polymers at the nanoscale, as a step toward the programmable assembly of advanced molecular channel materials.

A successful integration of functional molecular materials and devices requires electrodes with separation at the nanometer scale. This basic architecture can be realized in planar electrodes, yet their patterning often relies on low-throughput processes such as electron-beam lithography. The introduction of vertical nanogaps instead lends itself to low-cost wafer-scale fabrication. Channel widths can be precisely controlled by the thickness of a dielectric layer instead of being constrained by the diffraction limit of a photolithography system. We herein adopted the simplest vertical nanogap design, the etching of a metal-dielectric-metal stack, which has recently been used to demonstrate organic thin-film FETs that exhibited $I_{on}/I_{off} \sim 10^8$.[8] This type of electrode geometry is not intended for single-molecule device architectures but enables a reliable contacting of 10^2 to 10^3 molecules often required to achieve the necessary current levels in charge-based logic devices. Herein we describe the fabrication of dense arrays of vertical nanogaps with 50 nm separation on 6-in. wafers, using only standard microfabrication processes and materials. We selected Ru as the electrode metal (in contrast to more conventional Au and Pt commonly used in molecular

Received: May 16, 2024
Revised: July 9, 2024
Accepted: July 30, 2024
Published: August 6, 2024

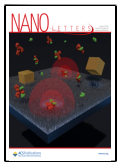

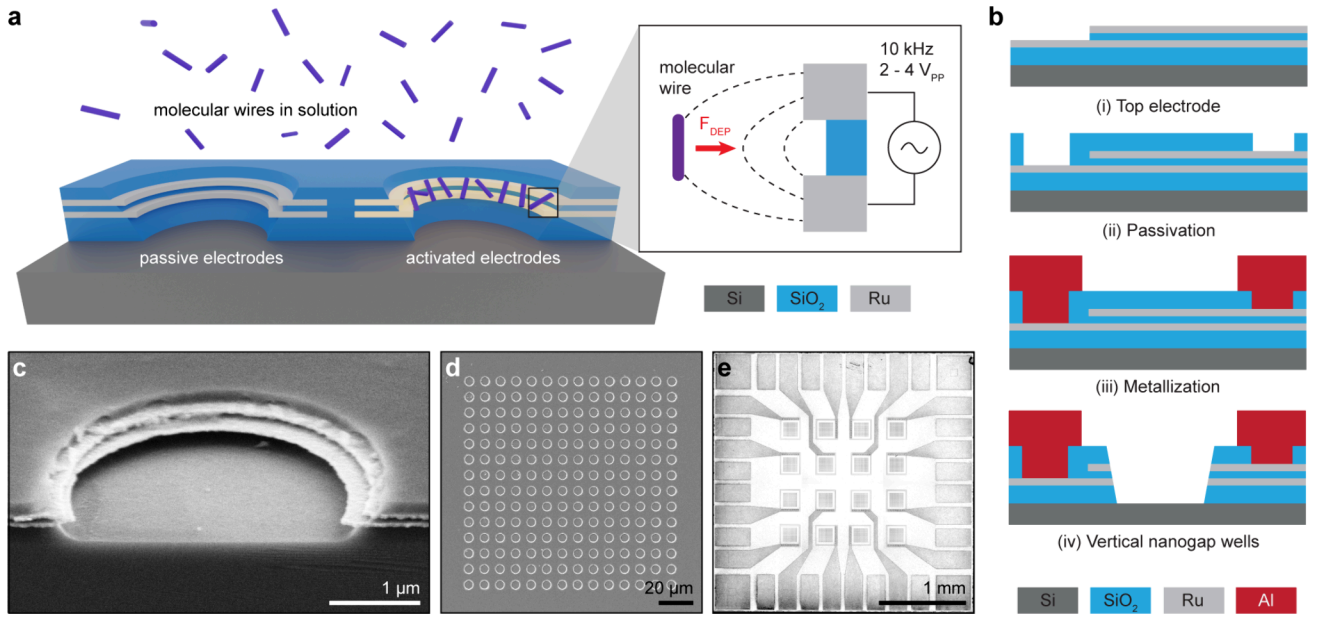

Figure 1. (a) Illustration of selective spatial localization of molecular wires at activated vertical nanogap electrodes via dielectrophoresis. (b) 4-mask fabrication flow of wafer-scale vertical nanogap electrodes. (c) Cross-section SEM image of a single vertical nanogap well. (d) Top-view SEM image of a well array. (e) Optical micrograph of a 9 mm^2 die showing 16 well arrays and Al routing and bond pads.

electronics) due to its low solid-state diffusivity and compatibility with dry etching, unique properties among the noble metals which are driving its use in next-generation CMOS interconnects.[9−11]

The manipulation of particles with electric fields involves a variety of effects, such as electrophoresis, dielectrophoresis (DEP), and electro-osmosis. Among these, the most suitable for manipulating quasi-one-dimensional particles intended as molecular channels is DEP, due to its ability to not only position but also orient particles across electrode gaps. Unlike electrophoresis and electro-osmosis, it does not require the presence of mobile ions. DEP has been successfully used to bridge μm-scale electrode gaps with metal nanowires[12,13] and carbon nanotubes (CNTs),[14−16] and to bridge nm-scale gaps with spherical nanoparticles[17,18] and polymer nanofibers.[19] Notably, it works with alternating current (AC) fields, which allows the use of capacitively coupled electrodes to achieve large-scale parallel assembly.[20] In DEP a nonuniform electric field, e.g. the fringe field at the edge of parallel-plate electrodes, polarizes nearby uncharged particles. The electrostatic interaction between the polarized particle, the medium, and the local field causes the particles to experience a DEP force. To compensate for ion migration, alternating current AC modulation with zero bias is applied. For an ellipsoidal particle aligned with the field, DEP theory gives the time-averaged force $\overline{F}$ as

$$\overline{F} = \alpha V \varepsilon_m \, \mathrm{Re}\left(\frac{\varepsilon_p^* - \varepsilon_m^*}{\varepsilon_m^*}\right) \nabla(\overline{E}^2) \tag{1}$$

where α is a shape factor, V is the volume of the ellipsoid, ε_m is the permittivity of the medium, ε_p^* and ε_m^* are the frequency-dependent complex permittivities of the particle and medium respectively, and $\overline{E}$ is the root-mean-square (rms) field strength.[21] In practice a multipole correction is included when the size of the particle approaches the electrode separation.[21] Adding to the complexity the polarizability of a solvated molecule depends on its local electrostatic environment,[22] rendering the evaluation of molecular DEP force nontrivial. Nonetheless, the assembly of single molecules into nanogap electrodes by low-voltage DEP and the measurement of electrical transport through the resulting devices has been demonstrated for DNA,[23] polypeptides,[24] and carbon nanotube-oligomer hybrids.[25] A key advantage to DEP is that any bridging molecule can be concentrated at the nanogaps from very dilute solutions,[24,25] overcoming one of the main challenges of undirected bridging with self-assembled monolayers.[26−28] This often represents a necessity for conductive polymers, which tend to be poorly soluble in many processing solvents.

The successful assembly and electrical characterization of molecular junction devices has shown that it is feasible to manipulate molecules in the size range of 10^1−10^2 kg mol^{-1} by DEP at low voltages but work on semiconducting molecules in scalable device architectures is lacking. We herein demonstrate the use of dense arrays of vertical nanogaps as dielectrophoretic electrodes, report for the first time the assembly of a low molecular weight (M_w = 20 kg mol^{-1}, confirmed by size exclusion chromatography, Supporting Information Figure S1) semiconducting polymer, polyaniline (PANI), from a dimethylformamide (DMF) solution, and measure appreciable conductance. We show that it is possible to selectively localize PANI at activated electrodes even if the entire device is exposed to a dilute solution of the polymer. In addition to electrical measurements, characterization by scanning electron microscopy (SEM), energy dispersive X-ray spectroscopy (EDX) and Raman spectroscopy support our conclusion. We emphasize here that nanoscale localization was achieved on a scalable device platform, fabricated with standard semiconductor materials and processes.

A schematic representation of the localization process, as well as the electrode geometry, is shown in Figure 1a. 50 nm vertical nanogap devices were fabricated on 6-in. Si wafers in four mask layers (Figure 1b). First, 200 nm SiO_2 was

https://doi.org/10.1021/acs.nanolett.4c02329
Nano Lett. 2024, 24, 10155−10160

deposited, followed by a stack of 50 nm Ru/50 nm SiO_2/50 nm Ru. The top Ru/SiO_2 layers were patterned to define the top electrodes. Second, a 200 nm SiO_2 passivation layer was deposited and patterned to open vias to the Ru electrode layers. Third, 1 μm Al was deposited and patterned to define the bonding pads and routing to the electrodes. Fourth, the vertical nanogaps were defined by patterning arrays of circles and etching through all the SiO_2 and Ru layers, forming vertical nanogaps along the circumference of each circular well. A short HF vapor etch was used to slightly recess the SiO_2 layers. Detailed fabrication procedures are provided in Supporting Information, Section II. The completed devices were diced and wire-bonded onto printed circuit boards for subsequent DEP experiments. Figure 1c shows a cross-section SEM image of a vertical nanogap well. The Ru electrodes (bright layers) are clearly separated by SiO_2 (dark layers), with a recess depth of approximately 50 nm. Electrical isolation between electrodes was confirmed by two-terminal resistance measurements. Vertical nanogaps with diameters ranging from 1 to 5 μm in 8 × 8 to 90 × 90 arrays (Figure 1d) were formed across different dies. In each array, nanogaps share the same pair of electrodes such that an array can be considered a single channel with a large effective width (circumference multiplied by the number of wells). The layout of the arrays, routing and bond pads was common to all dies (Figure 1e).

First, stable electrical connections between the test equipment and the well arrays of a die were verified by capacitance and resistance measurements. The capacitance of each array was found to be approximately 50 pF, which is in the expected range for the 210 × 210 μm electrodes. Contact and routing resistance was found to be less than 10 Ω and thus negligible. Then, for each die tested, two-terminal $I-V$ sweeps in the bias range ±1 V were performed at three different stages of processing (Figure 2a): first, on the as-fabricated die, before exposure to any chemicals; second, after the die had been exposed to a droplet of DMF while half the arrays were activated (V_{pp} = 2 V, 10 kHz sine wave applied); and third, after the die had been exposed to a droplet of 35 μg mL^{-1} PANI in DMF while half the arrays were activated. The arrays to be activated were randomly assigned at the first stage and the same arrays were activated through the second and third stages. It should be noted that the droplets covered the entire surface of the die and thus were in contact with all vertical nanogap arrays regardless of activation (Supporting Information Figure S2).

Figures 2b–e show the electrical characteristics of a representative die (array effective channel width 12.7 mm) at each stage. The as-fabricated arrays showed exponential $I-V$ curves and conductance values of ~10^{-9} S at 1 V bias; this leakage current is attributed to defect-assisted tunneling through the reactive-sputtered SiO_2 interlayer. After exposure to DMF, conductance values increased slightly but remained within 1 order of magnitude for both the activated and unactivated arrays. The overlapping conductance ranges for the two sets of arrays indicate that the activation signal does not interact with the solvent (DMF); subsequent changes in conductance can therefore be attributed to PANI alone. Indeed, after exposure to PANI, the conductance values of the activated arrays increased by 2 orders of magnitude, while the unactivated arrays showed no change. Measurements were recorded on multiple arrays after rinsing and drying of the dies. The increases in conductance of activated arrays following exposure to PANI and DEP are repeatable and statistically

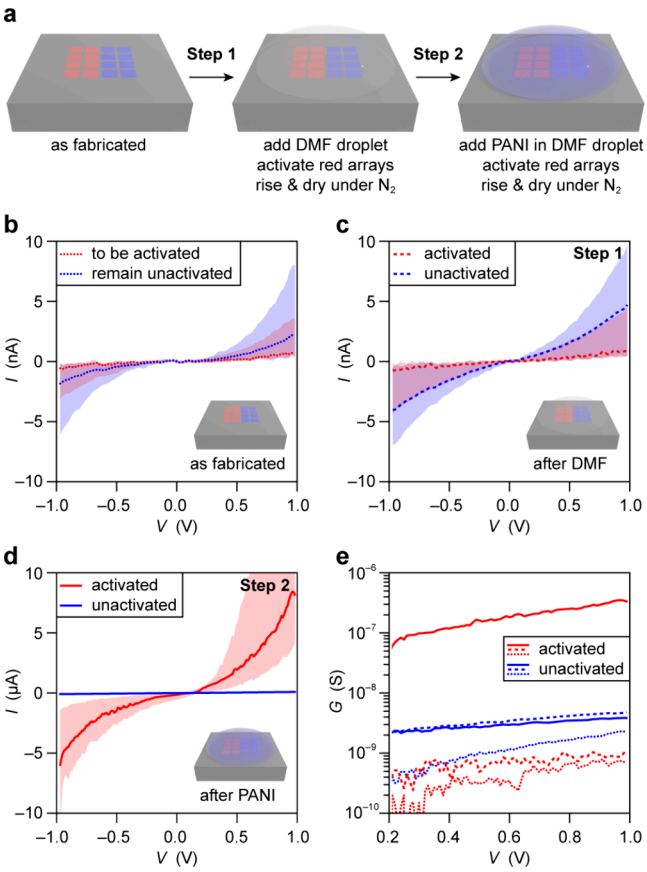

Figure 2. Two-terminal $I-V$ measurements of nanogap electrode arrays on a single die. (a) Schematic of the measurement sequence, from as-fabricated arrays to arrays exposed to DMF to arrays exposed to PANI. (b) $I-V$ curves of as-fabricated arrays. (c) $I-V$ curves of arrays after exposure to DMF (Step 1). (d) $I-V$ curves of arrays after exposure to PANI (Step 2). For (b–d), the solid lines represent the average of 6 arrays while the upper and lower bounds of the filled region represent the maximum and minimum, respectively. (e) Plot of conductance (G) against applied bias (V) of activated and unactivated arrays as fabricated, following sequential exposure to DMF (Step 1) and PANI (Step 2) (each curve represents the average of 6 arrays).

significant. This indicates that new stable conductance pathways have been selectively created between electrode pairs activated in the presence of PANI. The exponential $I-V$ curves are qualitatively similar to those observed for transport through conjugated oligomers.[28]

For SEM, EDX and Raman characterization, a set of DEP experiments were performed as detailed in the previous subsection, except that the activation potential was increased to 4 V. This resulted in more material being accumulated and thus better signal for these spectroscopic techniques. Figures 3a,b are top-view SEM images recorded on the same die at the edge of an unactivated and activated well, respectively. For the unactivated wells, the grain structures of the two Ru electrodes are clearly visible where they are exposed (bright layers); in contrast, the activated electrodes are covered in a thin, electron-translucent film that obscures the grain structure. This is also observed to a lesser extent for the devices activated at 2 V (Supporting Information Figure S4). These films were consistently observed in all wells of activated arrays but never in the wells of unactivated arrays (Supporting Information Figure S5), and are further evidence that additional

https://doi.org/10.1021/acs.nanolett.4c02329
Nano Lett. 2024, 24, 10155−10160

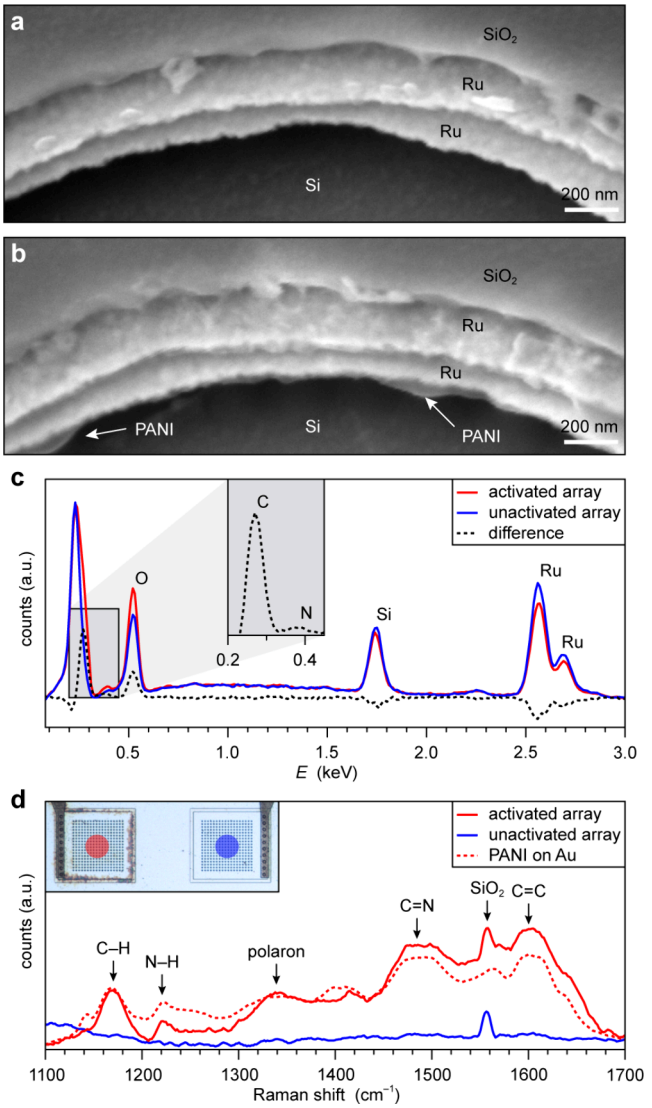

Figure 3. Scanning electron micrographs of wells exposed to PANI solution with (a) no potential and (b) 10 kHz, 4 V applied between the electrodes. The grain structure of Ru is clearly visible in the former, while "cobwebs" over the electrodes are apparent in the latter. (c) Energy-dispersive X-ray spectra of the exposed regions of the Ru electrodes, averaged over 5 points, showing excess C and N signals at the activated electrodes. (d) Low-magnification Raman spectra of arrays exposed to PANI solution with and without potential applied, compared to as-received PANI dropcast on a gold substrate. Inset: colored circles over arrays representing the approximate laser spot size used for spectroscopy. The activating potential was applied only to the left array.

conductance pathways have been formed between electrodes by the action of DEP.

The elemental composition of this assembled material was analyzed by EDX. Spectra were averaged over five points on the exposed electrode regions of both activated and unactivated wells, and are normalized to the Si peak (Figure 3c). A peak at 0.2 keV is attributed to low-energy transitions and could not be unambiguously assigned. Subtraction of the two spectra reveals a strong peak corresponding to C and a weaker signal attributed to N indicating that the assembled material is organic. The small differences in signals of O, Si, and Ru can be explained by the comparable sizes of the X-ray generation volume and the exposed Ru regions. For the 5 kV beam used, the X-ray generation volume is ∼100 nm, and depending on the precise beam location and sample drift over the integration time, more X-rays may be collected from the inside of the well (Si rich) or the outside (SiO_2, Ru rich) rather than the exposed electrode region.

The chemical structure of the assembled material was probed by Raman spectroscopy (532 nm excitation). As the exposed electrode region of a well is too small a target to focus a laser spot, the spectra were recorded at a low magnification, over the center of the well arrays, with a spot size of approximately 50 μm. The spectra obtained are thus an average over all the exposed surfaces of the array. Nevertheless, there is a clear difference between the spectra obtained from the activated versus unactivated array (Figure 3d). The spectrum from the activated array matches the reference spectrum taken of the source PANI solution drop-cast on an Au surface. The unactivated array has no discernible Raman signatures aside from SiO_2 (which is also seen in the spectrum of the activated array). The Raman peaks associated with PANI were assigned and match their reported spectra.[29] This result confirms that the selectively assembled material is indeed the emeraldine base form of PANI, and that it is chemically unchanged from that in the source solution.

Finally, to demonstrate that these molecular wire junction devices can be fabricated repeatably, we perform PANI DEP and $I-V$ measurements on five additional dies to extract an order of magnitude estimate of the conductivity of the assembled PANI. The chosen dies featured different well and array sizes and thus different effective channel widths. Figure 4

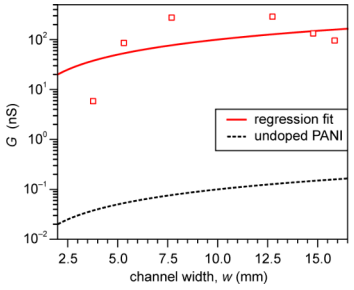

Figure 4. Scatter plot and constant conductivity fit of conductance against effective channel width for a set of 6 dies. The conductance curve for 10^{-10} S cm^{-1} conductivity, typical for undoped PANI, is shown for comparison.

shows that the average conductance (at 1 V bias) per array measured for each die are correlated with their effective channel widths, with slope on the order of 10^{-7} S cm^{-1}, 3 orders of magnitude greater than the bulk conductivity of undoped emeraldine base (10^{-10} S cm^{-1}), which is limited by interchain charge transfer. This increased conductivity could be due to unintended doping by residual moisture from the solvent, or a result of direct bridging of electrodes by PANI chains. However, the Raman spectrum of the assembled PANI shows none of the characteristic signatures associated with acid doping, such as an augmented C−C stretching band shifting to 1620 cm^{-1} or an augmented C−H bending band shifting to 1191 cm^{-1}.[30] On the other hand, the M_w of PANI used corresponds to a fully extended length of 92 nm,[31] and under the action of the localized high electric fields at the nanogap (2×10^7 V m^{-1}) during DEP, it is conceivable that PANI chains

https://doi.org/10.1021/acs.nanolett.4c02329
Nano Lett. 2024, 24, 10155−10160

adopt linear conformations that bridge the gap between both electrodes.

We have demonstrated that the combination of vertical nanogaps and AC electric fields can be used to selectively localize low molecular weight PANI in dense architectures. *I*–*V* measurements show that arrays with PANI assembled have 2 orders of magnitude increased conductance; SEM shows that the assembled material presents as electron-translucent film; and EDX and Raman spectroscopy confirmed the material to be PANI. This platform is a step toward scalable molecular electronic devices and could be applicable to more exotic 1D molecular channel materials, such as graphene nanoribbons.

■ ASSOCIATED CONTENT

Supporting Information

The Supporting Information is available free of charge at https://pubs.acs.org/doi/10.1021/acs.nanolett.4c02329.

Experimental details, materials and device characterization, and Figures S1–S4 (PDF)

■ AUTHOR INFORMATION

Corresponding Author

Felix R. Fischer − *Department of Chemistry, University of California, Berkeley, California 94720, United States; Materials Sciences Division, Lawrence Berkeley National Laboratory, Berkeley, California 94720, United States; Kavli Energy NanoSciences Institute at the University of California Berkeley and the Lawrence Berkeley National Laboratory, Berkeley, California 94720, United States; Bakar Institute of Digital Materials for the Planet, Division of Computing, Data Science, and Society, University of California, Berkeley, California 94720, United States;* orcid.org/0000-0003-4723-3111; Email: ffischer@berkeley.edu

Author

Han Xuan Wong − *Department of Chemistry, University of California, Berkeley, California 94720, United States*

Complete contact information is available at: https://pubs.acs.org/10.1021/acs.nanolett.4c02329

Author Contributions

All authors have given approval to the final version of the manuscript.

Notes

The authors declare no competing financial interest.

■ ACKNOWLEDGMENTS

This research program was generously supported by the Heising-Simons Faculty Fellows Program at UC Berkeley. H.X.W. acknowledges the Agency for Science, Technology, and Research (A*STAR) Singapore for support through the National Science Scholarship. All devices were fabricated at the UC Berkeley Marvell Nanofabrication Laboratory.

■ REFERENCES

(1) Zhao, M. Y.; Chen, Y. H.; Wang, K. X.; Zhang, Z. X.; Streit, J. K.; Fagan, J. A.; Tang, J. S.; Zheng, M.; Yang, C. Y.; Zhu, Z.; Sun, W. DNA-directed nanofabrication of high-performance carbon nanotube field-effect transistors. *Science* **2020**, *368*, 878−881.

(2) Bishop, M. D.; Hills, G.; Srimani, T.; Lau, C.; Murphy, D.; Fuller, S.; Humes, J.; Ratkovich, A.; Nelson, M.; Shulaker, M. M. Fabrication of carbon nanotube field-effect transistors in commercial silicon manufacturing facilities. *Nat. Electron.* **2020**, *3*, 492−501.

(3) Saraswat, V.; Jacobberger, R. M.; Arnold, M. S. Materials Science Challenges to Graphene Nanoribbon Electronics. *ACS Nano* **2021**, *15*, 3674−3708.

(4) Hwangbo, S.; Hu, L.; Hoang, A. T.; Choi, J. Y.; Ahn, J. H. Wafer-scale monolithic integration of full-colour micro-LED display using MoS_2 transistor. *Nat. Nanotechnol.* **2022**, *17*, 500−506.

(5) Yang, X. D.; Li, J.; Song, R.; Zhao, B.; Tang, J. M.; Kong, L. A.; Huang, H.; Zhang, Z. W.; Liao, L.; Liu, Y.; Duan, X. F.; Duan, X. D. Highly reproducible van der Waals integration of two-dimensional electronics on the wafer scale. *Nat. Nanotechnol.* **2023**, *18*, 471−478.

(6) Slota, M.; Keerthi, A.; Myers, W. K.; Tretyakov, E.; Baumgarten, M.; Ardavan, A.; Sadeghi, H.; Lambert, C. J.; Narita, A.; Müllen, K.; Bogani, L. Magnetic edge states and coherent manipulation of graphene nanoribbons. *Nature* **2018**, *557*, 691−695.

(7) Li, T. M.; Bandari, V. K.; Schmidt, O. G. Molecular Electronics: Creating and Bridging Molecular Junctions and Promoting Its Commercialization. *Adv. Mater.* **2023**, *35*, No. 2209088.

(8) Lenz, J.; del Giudice, F.; Geisenhof, F. R.; Winterer, F.; Weitz, R. T. Vertical, electrolyte-gated organic transistors show continuous operation in the MA cm^{-2} regime and artificial synaptic behaviour. *Nat. Nanotechnol.* **2019**, *14*, 579−585.

(9) Pedreira, O. V.; Croes, K.; Lesniewska, A.; Wu, C.; van der Veen, M. H.; de Messemaeker, J.; Vandersmissen, K.; Jourdan, N.; Wen, L. G.; Adelmann, C.; Briggs, B.; Gonzalez, V. V.; Bömmels, J.; Imec, Z. T. Reliability Study on Cobalt and Ruthenium as Alternative Metals for Advanced Interconnects. *IEEE International Reliability Physics Symposium (Irps)* **2017**, 6B-2.1−6B-2.8.

(10) Dutta, S.; Kundu, S.; Gupta, A.; Jamieson, G.; Granados, J. F. G.; Bömmels, J.; Wilson, C. J.; Tokei, Z.; Adelmann, C. Highly Scaled Ruthenium Interconnects. *IEEE Electr. Device. L.* **2017**, *38*, 949−951.

(11) Pedreira, O. V.; Stucchi, M.; Gupta, A.; Gonzalez, V. V.; van der Veen, M.; Lariviere, S.; Wilson, C. J.; Tokei, Z.; Croes, K. Metal reliability mechanisms in Ruthenium interconnects. *IEEE International Reliability Physics Symposium (Irps)* **2020**, 1−7.

(12) Smith, P. A.; Nordquist, C. D.; Jackson, T. N.; Mayer, T. S.; Martin, B. R.; Mbindyo, J.; Mallouk, T. E. Electric-field assisted assembly and alignment of metallic nanowires. *Appl. Phys. Lett.* **2000**, *77*, 1399−1401.

(13) Liu, Y. L.; Chung, J. H.; Liu, W. K.; Ruoff, R. S. Dielectrophoretic assembly of nanowires. *J. Phys. Chem. B* **2006**, *110*, 14098−14106.

(14) Stokes, P.; Khondaker, S. I. Local-gated single-walled carbon nanotube field effect transistors assembled by AC dielectrophoresis. *Nanotechnology* **2008**, *19*, No. 175202.

(15) Stokes, P.; Khondaker, S. I. High quality solution processed carbon nanotube transistors assembled by dielectrophoresis. *Appl. Phys. Lett.* **2010**, *96*, No. 083110.

(16) Zhang, Z. B.; Liu, X. J.; Campbell, E. E. B.; Zhang, S. L. Alternating current dielectrophoresis of carbon nanotubes. *J. Appl. Phys.* **2005**, *98*, No. 056103.

(17) Barik, A.; Chen, X. S.; Oh, S. H. Ultralow-Power Electronic Trapping of Nanoparticles with Sub-10 nm Gold Nanogap Electrodes. *Nano Lett.* **2016**, *16*, 6317−6324.

(18) Yu, E. S.; Lee, H.; Lee, S. M.; Kim, J.; Kim, T.; Lee, J.; Kim, C.; Seo, M.; Kim, J. H.; Byun, Y. T.; Park, S. C.; Lee, S. Y.; Lee, S. D.; Ryu, Y. S. Precise capture and dynamic relocation of nanoparticulate biomolecules through dielectrophoretic enhancement by vertical nanogap architectures. *Nat. Commun.* **2020**, *11*, 2804.

(19) Lin, Y. F.; Chen, C. H.; Xie, W. J.; Yang, S. H.; Hsu, C. S.; Lin, M. T.; Jian, W. B. Nano Approach Investigation of the Conduction Mechanism in Polyaniline Nanofibers. *ACS Nano* **2011**, *5*, 1541−1548.

(20) Vijayaraghavan, A.; Blatt, S.; Weissenberger, D.; Oron-Carl, M.; Hennrich, F.; Gerthsen, D.; Hahn, H.; Krupke, R. Ultra-large-scale directed assembly of single-walled carbon nanotube devices. *Nano Lett.* **2007**, *7*, 1556−1560.

(21) Pethig, R. Limitations of the Clausius-Mossotti function used in dielectrophoresis and electrical impedance studies of biomacromolecules. *Electrophoresis* **2019**, *40*, 2575−2583.
(22) Clarke, R. W.; Piper, J. D.; Ying, L. M.; Klenerman, D. Surface conductivity of biological macromolecules measured by nanopipette dielectrophoresis. *Phys. Rev. Lett.* **2007**, *98*, No. 198102.
(23) Porath, D.; Bezryadin, A.; de Vries, S.; Dekker, C. Direct measurement of electrical transport through DNA molecules. *Nature* **2000**, *403*, 635−638.
(24) Fuller, C. W.; Padayatti, P. S.; Abderrahim, H.; Adamiak, L.; Alagar, N.; Ananthapadmanabhan, N.; Baek, J.; Chinni, S.; Choi, C.; Delaney, K. J.; Dubielzig, R.; Frkanec, J.; Garcia, C.; Gardner, C.; Gebhardt, D.; Geiser, T.; Gutierrez, Z.; Hall, D. A.; Hodges, A. P.; Hou, G. Y.; Jain, S.; Jones, T.; Lobaton, R.; Majzik, Z.; Marte, A.; Mohan, P.; Mola, P.; Mudondo, P.; Mullinix, J.; Nguyen, T.; Ollinger, F.; Orr, S.; Ouyang, Y. X.; Pan, P.; Park, N.; Porras, D.; Prabhu, K.; Reese, C.; Ruel, T.; Sauerbrey, T.; Sawyer, J. R.; Sinha, P.; Tu, J.; Venkatesh, A. G.; VijayKumar, S.; Zheng, L.; Jin, S.; Tour, J. M.; Church, G. M.; Mola, P. W.; Merriman, B. Molecular electronics sensors on a scalable semiconductor chip: A platform for single-molecule measurement of binding kinetics and enzyme activity. *Proc. Natl. Acad. Sci. U. S. A.* **2022**, *119*, No. e2112812119.
(25) Marquardt, C. W.; Grunder, S.; Blaszczyk, A.; Dehm, S.; Hennrich, F.; von Löhneysen, H.; Mayor, M.; Krupke, R. Electroluminescence from a single nanotube-molecule-nanotube junction. *Nat. Nanotechnol.* **2010**, *5*, 863−867.
(26) Hashioka, S.; Saito, M.; Tamiya, E.; Matsumura, H. Deoxyribonucleic acid sensing device with 40-nm-gap-electrodes fabricated by low-cost conventional techniques. *Appl. Phys. Lett.* **2004**, *85*, 687−688.
(27) Iqbal, S. M.; Balasundaram, G.; Ghosh, S.; Bergstrom, D. E.; Bashir, R. Direct current electrical characterization of ds-DNA in nanogap junctions. *Appl. Phys. Lett.* **2005**, *86*, No. 153901.
(28) Sondergaard, R.; Strobel, S.; Bundgaard, E.; Norrman, K.; Hansen, A. G.; Albert, E.; Csaba, G.; Lugli, P.; Tornow, M.; Krebs, F. C. Conjugated 12 nm long oligomers as molecular wires in nanoelectronics. *J. Mater. Chem.* **2009**, *19*, 3899−3908.
(29) Bernard, M. C.; Hugot-Le Goff, A. Quantitative characterization of polyaniline films using Raman spectroscopy I: Polaron lattice and bipolaron. *Electrochim. Acta* **2006**, *52*, 595−603.
(30) Tao, S.; Hong, B.; Kerong, Z. An infrared and Raman spectroscopic study of polyanilines co-doped with metal ions and H. *Spectrochimica Acta Part A-Molecular and Biomolecular Spectroscopy* **2007**, *66*, 1364−1368.
(31) Lee, Y. H.; Chang, C. Z.; Yau, S. L.; Fan, L. J.; Yang, Y. W.; Yang, L. Y. O.; Itaya, K. Conformations of Polyaniline Molecules Adsorbed on Au(111) Probed by in Situ STM and ex Situ XPS and NEXAFS. *J. Am. Chem. Soc.* **2009**, *131*, 6468−6474.

https://doi.org/10.1021/acs.nanolett.4c02329
Nano Lett. 2024, 24, 10155−10160